ACS OMEGA

http://pubs.acs.org/journal/acsodf

Article

Raman Thermal Maturity of Coal and Type II Kerogen Based on Surface-Enhanced Raman Spectroscopy (SERS)

Yongbin Jin,* Sheng Wu, Li Gao, Chenyang Jiang, Fei Meng, and Yongchun Tang

Cite This: *ACS Omega* 2021, 6, 18504−18508

Read Online

ACCESS | Metrics & More | Article Recommendations

ABSTRACT: Low-maturity organic samples generate high levels of fluorescence during Raman detection. This fluorescence will obviously affect the Raman signals from organic matter. Our research shows that surface-enhanced Raman spectroscopy (SERS) can significantly enhance the ratio of the Raman signal from organic matter to the fluorescence background without changing the peak positions. This allows us to obtain more accurate Raman parameters for organic matter. In this study, we conducted Raman testing with SERS on coal and type II kerogen from the USA. We found that for both coal and type II kerogen, the exponential correlation between the thermal maturity and the distance between their D and G bands ($\Delta_{(G-D)}$) in the Raman spectra was good, and the *R*-squared values were 0.968 and 0.988, respectively. However, the Raman thermal maturity evolution curves for the coal and the type II kerogen were different. Compared with the Raman thermal maturity evolution curve of type II kerogen, that of coal was steeper. The two curves crossed each other at a $\Delta_{(G-D)}$ value of 223, which corresponds to a calculated vitrinite reflectance value of 0.61%. This study also shows that the Raman thermal maturity evolution model of organic matter is perhaps related mainly to its type.

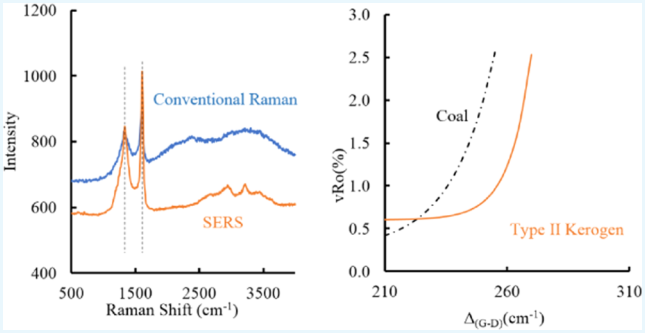

1. INTRODUCTION

In petroleum geology and coal petrography, the thermal maturity of organic matter is determined by optical inspection of vitrinite macerals, known as vitrinite reflectance.[1] This technique requires significant expertise and is labor-intensive.[2] Raman spectroscopy offers potential for rapid and non-destructive measurements to estimate the maturity of organic matter.[3−19] During thermal maturation, organic matter undergoes changes in the structure and composition, which results in variations in the carbon Raman spectra.[20] The main features of the Raman spectra of carbon are the so-called G and D bands, which lie at approximately 1585 and 1350 cm^{-1}, respectively, and are produced by the (Stokes) Raman scattering of light, typically induced by a 532 nm laser.[15]

The accurate quantification of Raman spectra by a systematic procedure is necessary to derive reliable spectral parameters that can then be compared between different operators and/or equipment setups. For low-maturity organic matter, the fluorescence background is usually predominant. The D and G bands in the Raman spectra are generally broad and can easily be confused with the fluorescence background.

Three visible excitation wavelengths were used in an attempt to reduce or eliminate the fluorescence background in spectra: 632.8, 514.5, and 457.9 nm. Measurements were carried out on three coal samples with vitrinite reflectance values (%νRo) of 1.16, 1.86, and 5.45%. None of the wavelengths fully removed the fluorescence background from any of these coal samples.[4] Although UV Raman spectroscopy is not dependent on fluorescence, two problems were encountered in tests with 244 nm UV excitation: the general shapes of the spectra were less sensitive to the coal maturity, and the samples were very unstable under laser irradiation.[4] We also found that low-maturity kerogen and coal (νRo < 1.2%) were easily burned in a 532 nm conventional Raman spectrometer, which increased the maturity of the organic matter.

SERS is a Raman spectroscopy (RS) technique that greatly enhances the Raman signals from the Raman-active analyte molecules that have been adsorbed onto certain specially prepared metal surfaces. It has been reported that increases in the intensity of Raman signals on the order of 10^4−10^6 have been regularly observed, with increases as high as 10^8 and 10^{14} for some systems.[21,22] SERS could provide an invaluable tool as a reliable, high-resolution detection technique for extremely minute quantities of target molecules, coupled with suppres-

Received: May 25, 2021
Accepted: June 30, 2021
Published: July 9, 2021

sion of fluorescence.[23] In this study, SERS was used to obtain more accurate Raman signals in the spectra of coal and kerogen.

2. RESULTS AND DISCUSSION

The structural evolution from low- to middle-maturity to high-maturity organic matter is similar to the evolution of a-C nanostructured graphite.[24] In the process, the Raman parameters, such as the positions of the G and D bands, will change as the maturity of organic matter increases. Table 1 lists the Raman results and the corresponding vitrinite reflectance (%νRo) values for the coal and the vitrinite reflectance equivalent (%VRE) for the type II kerogen. The positions of the G band and the D band of the coal shifted from 1568 to 1604 cm^{-1} and from 1349 to 1365 cm^{-1}, respectively, and the distance ($\Delta_{(G-D)}$) between the G and D bands shifted from 213 to 255 cm^{-1}, with a shift in the vitrinite reflectance values from 0.27 to 2.8%. The positions of the G band and the D band of the type II kerogen shifted from 1580 to 1605 cm^{-1} and from 1322 to 1358 cm^{-1}, respectively, and the $\Delta_{(G-D)}$ values shifted from 226 to 268 cm^{-1}, with VRE values from 0.55 to 2.15%. In general, the $\Delta_{(G-D)}$ values of the coal and the type II kerogen increased with their maturity evolution. The fitting curves of the reflectance vs the $\Delta_{(G-D)}$ values for the coal and the type II kerogen are shown in Figure 1. These values were best fitted by an exponential relationship, with R^2 values of 0.968 and 0.988 for coal and type II kerogen, respectively; the two curves can be described by the following equation

$$y = y_0 + A \times \exp(R_0 \times x) \quad (1)$$

In the equation, x represents the $\Delta_{(G-D)}$ value and y represents the calculated reflectance value. Substituting the fitting parameters of the coal and the type II kerogen into formula (1), the calculated reflectance value can be defined for the coal and the type II kerogen in this study as

$$\mathrm{Ram}_{coal}\% = 0.24835 + 8.38036 \times 10^{-7} \exp(0.05817 \times \Delta_{(G-D)}) \quad (2)$$

$$\mathrm{Ram}_{kerogenII}\% = 0.60055 + 1.20807 \times 10^{-13} \exp(0.1126 \times \Delta_{(G-D)}) \quad (3)$$

The Raman fitting curves for the coal and the type II kerogen are compared in Figure 2. The fitting curve for the coal shows a steeper trend than that for the type II kerogen. The two fitting curves cross each other at a $\Delta_{(G-D)}$ value of 223, which corresponds to a calculated reflectance value of 0.61%. Higher values indicate that the maturity of the coal is higher than that of the type II kerogen at the same $\Delta_{(G-D)}$ value.

Raman data of organic matter from different collection locations such as vitrinites and inertinites from the reference coal of Australia,[8] graptolite from the hot shale of the Silurian Qusaiba Formation in the Arabian Basin,[11] Woodford Shale of

Table 1. νRo Values, VRE Values, D and G Raman Band Positions, and $\Delta_{(G-D)}$ Values for the Coal and the Type II Kerogen

coal sample				
sample no.	νRo	D	G	$\Delta_{(G-D)}$
decs8	0.37	1359.8	1573.1	213.3
decs9	0.38	1356.2	1570.5	214.3
decs7	0.45	1365.5	1580.1	214.6
psoc1382p	0.52	1350.3	1568.5	218.2
decs5	0.59	1356.7	1578.2	221.5
decs15	0.80	1362.1	1588.1	226.0
decs29	1.00	1360.8	1593.9	233.1
decs3	1.28	1357.6	1596.5	238.9
psoc157	1.43	1353.8	1595.8	242.0
decs19	1.71	1351.6	1600.3	248.7
psoc1030	1.76	1350.1	1600.2	250.1
psoc881	1.95	1349.2	1600.5	251.3
psoc147	2.47	1350.1	1604.2	254.1
psoc1515	2.80	1349.4	1604.4	255.0
type II kerogen				
sample no.	VRE	D	G	$\Delta_{(G-D)}$
W-1	0.55	1358.4	1584.2	225.8
W-2	0.58	1351.2	1580.6	229.4
W-3	0.65	1357.9	1591.3	233.4
W-4	0.75	1344.8	1585.1	240.3
W-5	0.83	1356.1	1605.3	249.2
W-6	1.10	1345.2	1603.1	257.9
W-7	1.16	1339.9	1600.3	260.4
W-8	1.60	1329.2	1593.4	264.2
W-9	2.15	1321.8	1590.2	268.4

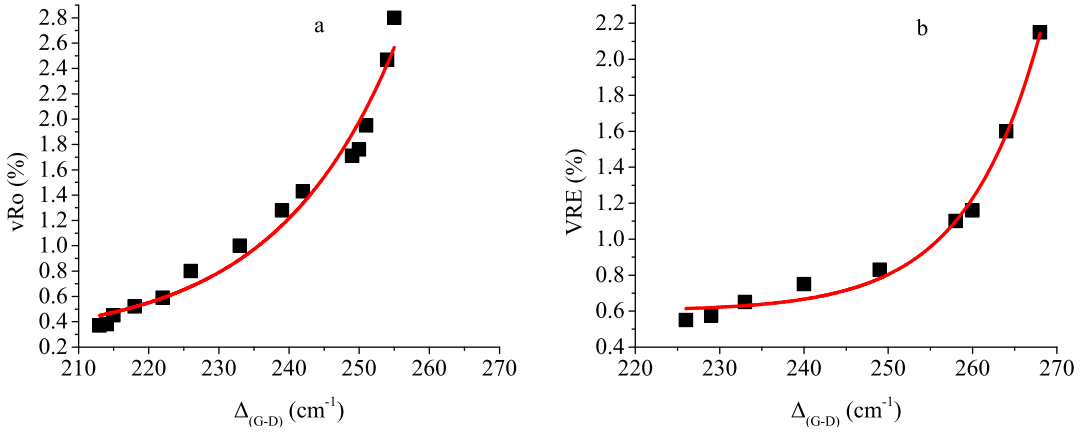

Figure 1. Fitting mode for the data from coal (a) and type II kerogen (b).

https://doi.org/10.1021/acsomega.1c02730
ACS Omega 2021, 6, 18504−18508

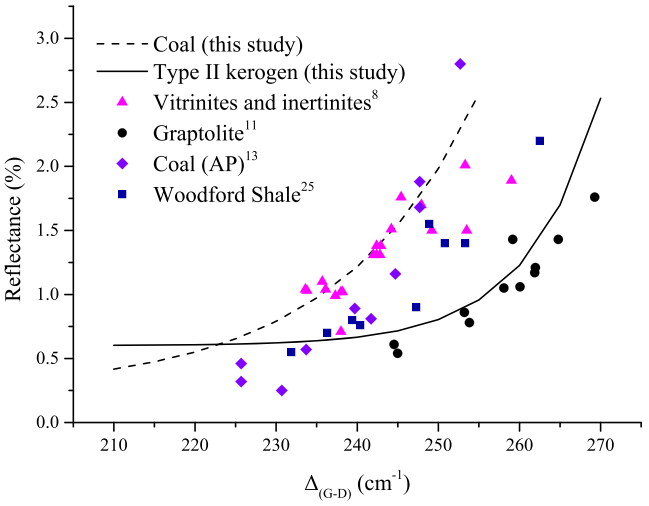

Figure 2. Comparison of the fitting curves of reflectance values vs $\Delta_{(G-D)}$ for the coal and the type II kerogen got in this study and the results for vitrinites and inertinites from the reference coal of Australia,[8] graptolite (corrected to 532 nm) from the hot shale of the Silurian Qusaiba Formation in the Arabian Basin,[11] Woodford Shale of Oklahoma[13] (corrected to 532 nm), and coal from AP[25] (corrected to 532 nm).

the state of Oklahoma,[25] and coal of the Argonne Premium coal bank (AP)[13] were acquired for comparison (Figure 2). The fitting curves of the coal and the type II kerogen of this study are also shown in Figure 2. Only data for reflectance value <3% are shown in Figure 2, as this covers the range of coal and type II kerogen of our study. The hydrogen and oxygen indices of graptolite are similar to those of type II kerogen[26], which means that graptolite can represent type II kerogen in thermal maturity. Except for vitrinite and inertinite, the Raman data of graptolite, Woodford Shale, and coal of AP were obtained at 632.8 nm. The D band position in the Raman spectrum of organic matter is dependent on the excitation wavelength. Schmidt Mumm and İnan[11] also reported that the D band positions of a graptolite obtained at the excitation wavelengths of 488, 633, and 788 nm were 1320, 1332, and 1338 cm^{-1}, respectively. On fitting these three points, we got a second-order equation with an *R*-squared value of 1

$$y = -0.0001x^2 + 0.2474x + 1234.3 \quad (4)$$

In this equation, y represents the D band position and x represents the excitation wavelength. The D band position obtained at 632.8 nm can be recalculated for the excitation wavelength of 532 nm used in our study. The dispersion in the D band position was 7.7 cm^{-1} between 632.8 and 532 nm, and when this adjustment was applied, we obtained the $\Delta_{(G-D)}$ values of organic matter at 532 nm. The Raman data for vitrinite and inertinite from the reference coal of Australia[8] are distributed along the curve for the coal of our study. However, the Raman data for graptolites from the hot shale of the Silurian Qusaiba Formation in the Arabian Basin[11] are distributed along the curve for the type II kerogen in this study (Figure 2). The data of Woodford Shale and coal of AP, respectively, do not fit well with the type II kerogen curve and coal seam curve obtained in this study in Figure 2. In conventional Raman spectroscopy, fluorescence is obvious for low-maturity organic matter. Fluorescence can raise and tilt the baseline of the D and G bands, which may change the shape and position of the D and G bands. Clay minerals in shale, such as kaolin, also emit high fluorescence in the Raman spectrum. Kerogen extraction can reduce the influence of the fluorescence of clay minerals on the D and G bands. Organic matter such as coal and kerogen are more easily degraded in Raman measurements. If the excitation intensity is reduced, the D and G band signals will be weakened. When a coolant such as water is added to the sample, the excitation intensity can be increased without burning the organic matter. The homogeneity of the sample also has an impact on the Raman data of the organic matter. Organic matter of different maturities is unevenly distributed in a coal or shale sample. When the sample is ground into powder, the accuracy of the organic Raman data will be improved. We believe that their Raman detection method causes some data of Woodford Shale and coal of AP to not fit well with the type II kerogen curve and the coal curve obtained in this study. The graptolite data fits well with the type II kerogen curve obtained in this study, which may be due to some measures taken to reduce the fluorescence emission of graptolite.[11] In general, the correlation of thermal maturity with $\Delta_{(G-D)}$ values for the coal was obviously different from that for the type II kerogen. This difference is perhaps related to only the type of organic matter and not to the sample collection location.

3. CONCLUSIONS

SERS can obviously enhance the signals of the D and G bands from organic matter and quench the fluorescence background in the Raman spectrogram, which enables more accurate Raman parameters to be obtained for low-maturity organic matter.

Although the thermal maturity of the coal and the type II kerogen had an exponential relationship with the Raman parameters, in the graph of thermal maturity vs $\Delta_{(G-D)}$ values, the Raman maturity curves for the coal and the type II kerogen were distributed in different regions.

On the basis of comparing the Raman maturity of graptolite from the Middle East and reference coal from Australia with that of the coal and the type II kerogen from the USA used in this study, we believe that the Raman-based maturity evolution of organic matter is perhaps mainly related to its type and not the location of sample collection. This shows that Raman technology can be a powerful tool for studying the thermal maturity of organic matter.

4. SAMPLES AND EXPERIMENTS

4.1. Samples. Coal samples were purchased from the Coal Sample Bank of Earth and Mineral Sciences (EMS) Energy Institute, Pennsylvania State University. The maturity and other aspects of the geological background of these coal samples can be found on the EMS Energy Institute website. Type II kerogen samples were extracted from Woodford Shale.

4.2. Ag Nanoparticle Preparation. In this study, the SERS measurement of coal and type II kerogen was carried out using Ag nanoparticles prepared by a chemical reduction technique reported previously[27]

$$AgNO_3 + NaBH_4 \rightarrow Ag + 1/2H_2 + 1/2\ B_2H_6 + NaNO_3 \quad (5)$$

The silver nitrate (>99% $AgNO_3$) and sodium borohydride (99% NaBH4) used in the experiment were purchased from Sigma-Aldrich Chemical Company. A 10 mL volume of 1.0 mM silver nitrate was added dropwise to 30 mL of 2.0 mM

https://doi.org/10.1021/acsomega.1c02730
ACS Omega 2021, 6, 18504−18508

sodium borohydride solution that had been chilled in an ice bath. The reaction mixture was stirred vigorously on a magnetic stir plate. The Ag nanoparticle colloidal solution was bright yellow when all of the silver nitrate had been added. The colloidal solution was stable at room temperature and could be stored for more than 1 year. The size of the Ag nanoparticles in the colloidal solution was measured at the South China University of Technology using a HORIBA Scientific SZ-100 nanoparticle analyzer; the size was 15.5−21.2 nm initially and 38.6∼42 nm after 1 year of storage. When irradiated by a 532 nm laser in conventional Raman spectroscopy, the low-maturity organic sample emitted a weak signal and was highly fluorescent. We conducted comparative tests on coal and type II kerogen using conventional Raman spectroscopy and SERS in this study. Figure 3 shows the comparison of low-maturity a coal sample

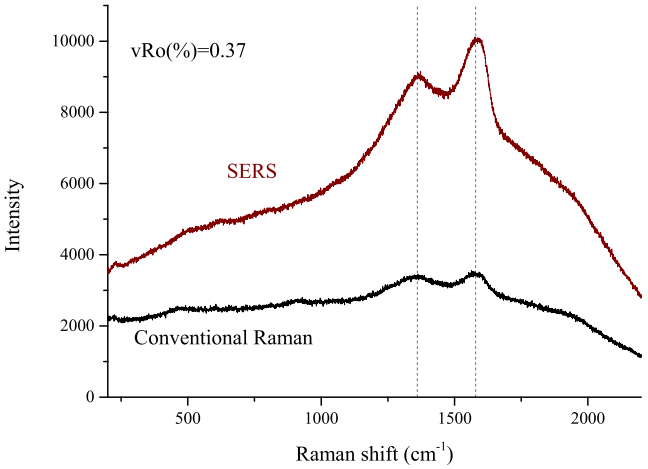

Figure 3. Comparison of the SERS spectra with the conventional Raman spectra of the D and G bands of a coal sample (νRo% = 0.37).

(νRo% = 0.37). The D band was flat and the G band was very small in conventional Raman spectroscopy. It is difficult to identify the precise positions of the D and G bands for low-maturity coal samples. However, in SERS, the D and G bands were significantly enhanced, and the ratio of the band height to the half-width was different. The two bands were higher and their shape was sharper. This showed that SERS can be used to obtain the accurate positions of the D and G bands for low-maturity organic matter. Our study showed that the positions of the D and G bands were not changed on comparing SERS with the conventional Raman spectra (Figure 3).

Before the coal samples were analyzed using a Raman spectrometer, they were ground to ∼150 mesh powder using an agate mortar. Approximately 20 mg of the sample powder to be measured in the Raman spectrometer was loaded onto a rough copper plate and spread into a thin layer of approximately 1 mm in thickness. Then, 2−3 drops of the colloidal solution of Ag nanoparticles were added to the sample powder while ensuring that the sample powder was completely covered by the colloidal solution of Ag nanoparticles.

4.3. Raman Measurements. The Raman experiments of coal and type II kerogen were performed at the Power, Environmental and Energy Research Institute using a Raman spectrometer designed on the basis of an ASEQ instruments HR1 Raman spectrometer (ASEQ instruments, Vancouver, Canada) for studying the thermal maturity evolution of organic matter. The spectrometer was equipped with a 10× lens and a laser source with a 532 nm excitation wavelength. The sealed charge-coupled device (CCD) detector was maintained at −40 °C using a semiconductor cooler to ensure that background noise was as low as possible. Each sample was scanned 3−5 times, and the exposure time for each scan was 5 s. The reflectance values and the Raman data of the coal and the type II kerogen are listed in Table 1.

AUTHOR INFORMATION

Corresponding Author

Yongbin Jin − *Key Laboratory of Ocean and Marginal Sea Geology, South China Sea Institute of Oceanology, Innovation Academy of South China Sea Ecology and Environmental Engineering, Chinese Academy of Sciences, Guangzhou 510301, China; Southern Marine Science and Engineering Guangdong Laboratory (Guangzhou), Guangzhou 5111458, China; Power, Environmental and Energy Research Institute, Covina, California 91722, United States;* orcid.org/0000-0002-8010-2757; Email: jingeyb@gmail.com

Authors

Sheng Wu − *Power, Environmental and Energy Research Institute, Covina, California 91722, United States*

Li Gao − *Power, Environmental and Energy Research Institute, Covina, California 91722, United States*

Chenyang Jiang − *Power, Environmental and Energy Research Institute, Covina, California 91722, United States*

Fei Meng − *Power, Environmental and Energy Research Institute, Covina, California 91722, United States*

Yongchun Tang − *Power, Environmental and Energy Research Institute, Covina, California 91722, United States*

Complete contact information is available at: https://pubs.acs.org/10.1021/acsomega.1c02730

Notes

The authors declare no competing financial interest.

ACKNOWLEDGMENTS

The authors are grateful to the supplier for providing the type II kerogen samples. The work was financially supported by the National Natural Science Foundation of China (41773039, 41706045, U1901217, 41876052), Key Special Project for Introduced Talents Team of Southern Marine Science and Engineering Guangdong Laboratory (Guangzhou) (GML2019ZD0104), Special Support Program for Cultivating High-level Talents in Guangdong Province (2019BT02H594), the open research fund of State Key Laboratory of Geomechanics and Geotechnical Engineering, Institute of Rock and Soil Mechanics, Chinese Academy of Sciences (Z0190915), and CAS Open Fund of the Key Laboratory of Marine Geology and Environment (MGE2018KG14).

REFERENCES

(1) Diessel, C. F. K.; Brothers, R. N.; Black, P. M. Coalification and graphitisation in high-pressure schists inNew Caledonia. *Contrib. Mineral. Petrol.* **1978**, *68*, 63−78.

(2) Hackley, P. C.; Araujo, C. V.; Borrego, A. G.; Bouzinos, A.; Cardott, B. J.; Cook, A. C.; Eble, C.; Flores, D.; Gentzis, T.; Gonçalves, P. A.; Mendonça Filho, J. G.; Hámor-Vidó, M.; Jelonek, I.; Kommeren, K.; Knowles, W.; Kus, J.; Mastalerz, M.; Menezes, T. R.; Newman, J.; Oikonomopoulos, I. K.; Pawlewicz, M.; Pickel, W.;

https://doi.org/10.1021/acsomega.1c02730
ACS Omega 2021, 6, 18504−18508

Potter, J.; Ranasinghe, P.; Read, H.; Reyes, J.; De La Rosa Rodriguez, G.; Alves Fernandes de Souza, I. V.; Suárez-Ruiz, I.; Sýkorová, I.; Valentine, B. J. Standardization of reflectance measurements in dispersed organic matter: Results of an exercise to improve interlaboratory agreement. *Mar. Pet. Geol.* **2015**, *59*, 22−34.
(3) Beyssac, O.; Goffé, B.; Chopin, C.; Rouzaud, J. N. Raman spectra of carbonaceous material in metasediments: a new geothermometer. *J. Metamorph. Geol.* **2002**, *20*, 859−871.
(4) Quirico, E.; Rouzaud, J.-N.; Bonal, L.; Montagnac, G. Maturation grade of coals as revealed by Raman spectroscopy: progress and problems. *Spectrochim. Acta, Part A* **2005**, *61*, 2368−2377.
(5) Lahfid, A.; Beyssac, O.; Deville, E.; Negro, F.; Chopin, C.; Goffe, B. Evolution of the Raman spectrum of carbonaceous material in low-grade metasediments of the Glarus Alps (Switzerland). *Terra Nova* **2010**, *22*, 354−360.
(6) Guedes, A.; Valentim, B.; Prieto, A. C.; Rodrigues, S.; Noronha, F. Micro-Raman spectroscopy of collotelinite, fusinite and macrinite. *Int. J. Coal Geol.* **2010**, *83*, 415−422.
(7) Hinrichs, R.; Brown, M. T.; Vasconcellos, M.A.Z.; Abrashev, M. V.; Kalkreuth, W. Simple procedure for an estimation of the coal rank using micro-Raman spectroscopy. *Int. J. Coal Geol.* **2014**, *136*, 52−58.
(8) Wilkins, R. W. T.; Boudou, R.; Sherwood, N.; Xiao, X. M. Thermal maturity evaluation from inertinites by Raman spectroscopy: The 'RaMM' technique. *Int. J. Coal Geol.*. **2014**, *128-129*, 143−152.
(9) Zhou, Q.; Xiao, X.; Pan, L.; Tian, H. The relationship between micro-Raman spectral parameters and reflectance of solid bitumen. *Int. J. Coal Geol.* **2014**, *121*, 19−25.
(10) Lünsdorf, N. K. Raman spectroscopy of dispersed vitrinite - methodical aspects and correlation with reflectance. *Int. J. Coal Geol.* **2016**, *153*, 75−86.
(11) Schmidt Mumm, A.; İnan, S. Microscale organic maturity determination of graptolites using Raman spectroscopy. *Int. J. Coal Geol.* **2016**, *162*, 96−107.
(12) Ferralis, N.; Matys, E. D.; Knoll, A. H.; Hallmann, C.; Summons, R. E. Rapid, direct and non-destructive assessment of fossil organic matter via micro-Raman spectro-scopy. *Carbon* **2016**, *108*, 440−449.
(13) Kelemen, S. R.; Fang, H. L. Maturity trends in Raman spectra from kerogen and coal. *Energy Fuels* **2001**, *15*, 653−658.
(14) Liu, D.; Xiao, X.; Tian, H.; Min, Y.; Zhou, Q.; Cheng, P.; Shen, J. Sample maturation calculated using Raman spectroscopic parameters for solid organics: methodology and geological applications. *Chin. Sci. Bull.* **2013**, *58*, 1285−1298.
(15) Marshall, C. P.; Edwards, H.G.M.; Jehlicka, J. Understanding the application of Raman spectroscopy to the detection of traces of life. *Astrobiology* **2010**, *10*, 229−243.
(16) Pasteris, J. D.; Wopenka, B. Raman spectra of graphite as indicators of degree of metamorphism. *Can. Mineral.* **1991**, *29*, 1−9.
(17) Spötl, C.; Houseknecht, D. W.; Jaques, R. C. Kerogen maturation and incipient graphitization of hydrocarbon source rocks in the Arkoma Basin, Oklahoma and Arkansas: a combined petrographic and Raman spectrometric study. *Org. Geochem.* **1998**, *28*, 535−542.
(18) Tuinstra, F.; Koenig, J. Raman spectrum of graphite. *J. Chem. Phys.* **1970**, *53*, 1126−1130.
(19) Yui, T.-F.; Huang, E.; Xu, J. Raman spectrum of carbonaceous material: a possible metamorphic grade indicator for low-grade metamorphic rocks. *J. Metamorph. Geol.* **1996**, *14*, 115−124.
(20) Tissot, B. P.; Welte, D. H. *Petroleum Formation and Occurence*, 2. rev. and enl. ed.; Springer: Berlin, Heidelberg, 1984.
(21) Kneipp, K.; Kneipp, H.; Itzkan, I.; Dasari, R. R.; Feld, M. S. Ultrasensitive chemical analysis by Raman spectroscopy. *Chem Rev.* **1999**, *9910*, 2957−2976.
(22) Moskovits, M. Surface-enhanced spectroscopy. *Rev. Mod. Phys.* **1985**, *57*, 783−862.
(23) Lombardi, J. R.; Birke, R. L. A Unified View of Surface-Enhanced Raman Scattering. *Acc. Chem. Res.* **2009**, *42*, 734−742.
(24) Ferrari, A. C.; Robertson, J. Interpretation of Raman spectra of disordered and amorphous carbon. *Phys. Rev. B.* **2000**, *61*, 14095−14107.
(25) Seyedalireza, K.; Abarghani, A.; Liu, K. Q.; Guedes, A.; Valentim, B.; Ostadhassan, M. Backtracking to Parent Maceral from Produced Bitumen with Raman Spectroscopy. *Minerals* **2020**, *10*, No. 679.
(26) Bustin, R. M.; Link, C.; Goodarzi, F. Optical properties and chemistry of graptolite periderms following laboratory simulated maturation. *Org. Geochem.* **1989**, *14*, 355−364.
(27) Solomon, S. D.; Bahadory, M.; Jeyarajasingam, A. V.; Rutkowsky, S. A.; Boritz, C.; Mulfinger, L. Synthesis and Study of Silver Nanoparticles. *J. Chem. Educ.* **2007**, *84*, 322−325.

https://doi.org/10.1021/acsomega.1c02730
ACS Omega 2021, 6, 18504−18508